A&A 460, 125–131 (2006)
DOI: 10.1051/0004-6361:20054784

Astronomy & Astrophysics

Diagnostics of SS433 with the RXTE

E. Filippova[1,2], M. Revnivtsev[1,2], S. Fabrika[3], K. Postnov[4], and E. Seifina[4]

[1] Max-Planck-Institute für Astrophysik, Karl-Schwarzschild-Str. 1, 85740 Garching bei München, Germany
[2] Space Research Institute, Russian Academy of Sciences, Profsoyuznaya 84/32, 117997 Moscow, Russia
e-mail: kate@hea.iki.rssi.ru
[3] Special Astrophysical Observatory, Nizhnij Arkhyz, Karachaevo-Cherkesiya 369167, Russia
[4] Sternberg Astronomical Institute, 119992 Moscow, Russia

Received 28 December 2005 / Accepted 24 August 2006

ABSTRACT

We present our analysis of the extensive monitoring of SS433 by the RXTE observatory collected over the period 1996–2005. The difference between energy spectra taken at different precessional and orbital phases shows the presence of strong photoabsorption ($N_{\rm H} > 10^{23}\,{\rm cm}^{-2}$) near the optical star, probably due to its powerful, dense wind. Therefore the size of the secondary deduced from analysis of X-ray orbital eclipses might be significantly larger than its Roche lobe size, which must be taken into account when evaluating the mass ratio from analysis of X-ray eclipses. Assuming that a precessing accretion disk is geometrically thick, we recover the temperature profile in the X-ray emitting jet that best fits the observed precessional variations in the X-ray emission temperature. The hottest visible part of the X-ray jet is located at a distance of $l_0/a \sim 0.06{-}0.09$, or $\sim 2{-}3 \times 10^{11}$ cm from the central compact object, and has a temperature of about $T_{\rm max} \sim 30$ keV. We discovered appreciable orbital X-ray eclipses at the "crossover" precessional phases (jets are in the plane of the sky, disk is edge-on), which under model assumptions put a lower limit on the size of the optical component $R/a \gtrsim 0.5$ and an upper limit on a mass ratio of binary companions $q = M_{\rm x}/M_{\rm opt} \lesssim 0.3{-}0.35$, if the X-ray opaque size of the star is not larger than $1.2R_{\rm Roche,secondary}$.

Key words. accretion, accretion disks – black hole physics – binaries: eclipsing – X-rays: binaries – radiation mechanisms: general

1. Introduction

The source SS433 is the only Galactic X-ray binary with X-ray emission from optically thin thermal plasma originating in hot jets outflowing with a sub-relativistic velocity of 0.26 c. The binary system is thought to consist of a compact object (probably a black hole) accreting matter at a super-Eddington rate from a high-mass star filling its Roche lobe (Margon 1984; Cherepaschuk 2002; see Fabrika 2004, for a recent review). Apparently, the innermost accretion flow and the supercritical accretion disk wind completely screen the region of the main energy release, and most of the energy from SS433 is observed in the optical and UV (Cherepashchuk et al. 1982; Dolan et al. 1997).

The system demonstrates a complex variability including periodicities – the precessional (~162 days), orbital (~13 days), and nutational (nodding, ~6 days) periods – which can be used to tightly constrain the binary system parameters. In particular, the kinematical model of the system leads to a binary inclination angle of $i \sim 78.05°$, and the jet precession angle is ~20.92° (Fabrika 2004).

Mildly relativistic ($v \sim 0.26c$) jets launched in the vicinity of the compact object consist of protons and electrons ("heavy" jet) with a high temperature (1–30 keV). Plasma moving along the jet gradually cools down so that, at distances $\sim 10^{13}{-}10^{14}$ cm from the central object, a thermal instability develops and clumps start forming. At distances $10^{14}{-}10^{15}$ cm, the temperature of matter drops to $\sim 2 \times 10^4$ K so that optical line emission appears. At larger distances the jets shine in the radio diapason.

The main properties of the X-ray emission observed from SS433 can be summarized as follows:

- the X-ray emission mechanism is thermal bremsstrahlung radiation (e.g. Marshall et al. 1979; Watson et al. 1986; Matsuoka et al. 1986; Brinkmann et al. 1991). Based on measurements of the doppler shifts of the emission lines from the thermal plasma, it is believed that the total (or majority of) the X-ray emission originates in the jets (Fabrika 2004);
- the temperature of optically thin plasma decreases along the jet. The hottest regions near the jet base have temperatures up to ~20–30 keV (e.g. Kotani et al. 1996; Marshall et al. 2002; Cherepashchuk et al. 2003; Namiki et al. 2003);
- a detailed study of X-ray emission lines in SS433 shows that the full opening angle of the jet should be very small, not larger than ~1–2°. Such an opening angle roughly corresponds to free expansion of the jet material in the direction perpendicular to the jet motion (Marshall et al. 2002; Namiki et al. 2003);
- there are X-ray eclipses caused by the donor star. The temperature of the observed radiation drops significantly during the eclipse, and the depth of the eclipse increases at high energies (Stewart et al. 1987; Kawai et al. 1989; Brinkmann et al. 1991);
- precession of the geometrically thick accretion disk is accompanied by strong variations in both temperature and the flux of X-ray emission (Yuan et al. 1995). Amplitudes of precessional and orbital variations in X-ray emission strongly increase with energy (e.g. Cherepashchuk et al. 2005). The precession variations are likely to be due to

partial eclipse of the X-ray jets by the thick precessing accretion disk.

Over the life time of the RXTE observatory many observations of SS433 were performed at different precessional and orbital phases (see e.g. Gies et al. 2002b; Nandi et al. 2005). The relatively complete sampling of the source at different orbital and precessional phases provides us with an opportunity to perform a tomographic study of the X-ray jet in SS433. Examining of orbital eclipses (caused by the optical star) and precessional variability (caused by the geometrically thick accretion disk) allows us to separate contributions of different parts of the jet to the total X-ray emission.

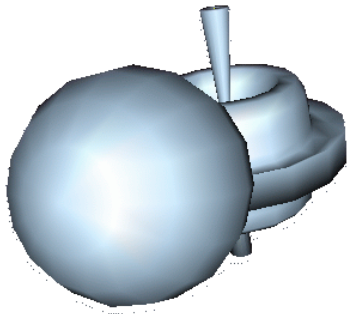

Fig. 1. Scheme of the X-ray binary SS433. Both the optical component and geometrically-thick accretion disk can eclipse central parts of the X-ray jet.

2. Observations and data analysis

In this paper, we have used all publicly available data of the RXTE observatory obtained from April 1996 until August 2004 and also the results of our dedicated SS433 observations during RXTE AO10 (P91103). In total, this includes 100 observations taken at different precessional and orbital phases of the system. We used precessional and orbital ephemeris furnished by Fabrika (2004). We adopted the following parameters of the system: the moment of the maximum emission-line separation (T3) $T_3 = 2\,443\,507.47$ JD, the precessional period $P_{\rm prec} = 162.375$ days, the orbital period $P_{\rm orb} = 13.08211$ days, the moment of the primary optical eclipse $T_0 = 2\,450\,023.62$ JD. For nutational periodicity, we adopted $P_{\rm nut} = 6.2877$ days, the moment of maximum brightness in V band due to the nodding variability $T_{0,\rm nut} = 2\,450\,000.94$ JD, and the nodding amplitude 2.8°.

Standard tasks of the LHEASOFT/FTOOLS 5.3.1 package were utilized for data processing. For accurate background modeling of the PCA spectrometer of the RXTE observatory, we applied the "L7_240CM" faint model (see e.g. Jahoda et al. 2006). Only spectra obtained by the PCU2 detector were used for the analysis. To construct broad-band spectra, we also used data from HEXTE detectors.

3. Variation in X-ray emission over precessional and orbital periods

The binary system is schematically shown in Fig. 1. The binary separation is assumed to be $a \sim 4 \times 10^{12}$ cm (e.g. Hillwig et al. 2004). The mass ratio of the companions is still not well-constrained and varies in different works from $q = M_{\rm x}/M_{\rm opt} \sim 0.2$ to $q \sim 0.6$ (Antokhina et al. 1992; Gies et al. 2002a). However, the latest studies of the kinematics of the binary system favor a smaller mass ratio $q \sim 0.2{-}0.3$ (Hillwig et al. 2004; Cherepashchuk et al. 2005).

After discovery of the donor-star absorption spectrum in the blue spectral region of SS433 (Gies et al. 2002a), there were several contradictory results for the orbital behavior of the absorption lines. From our experience with spectral studies of these absorption lines (Cherepashchuk et al. 2005), we may conclude that there are two important restrictions, hand by adhering to them one may hope to detect "real donor-star" absorption lines.

1. Observations must be performed in the precessional phases of the most open accretion disk ($\psi \sim 0$), when the disk outflow does not intersect the line of sight. The observations by Gies et al. (2002a), Hillwig et al. (2004) and Cherepashchuk et al. (2005) satisfy this condition.

2. Only the weakest absorption lines have to be taken into account, while stronger lines will trace the gas streams in the binary even at precessional phases $\psi \sim 0$, because of the huge ($\sim 10^{-4}$ $M_\odot$/yr) mass transfer rate in SS433 (Fabrika 2004). In the commonly used cross-correlation method, the strongest Fe II absorption lines in the studied spectral region will dominate and distort the radial velocity curves (Hillwig et al. 2004; Barnes et al. 2006). The observations by Gies et al. (2002a) and Cherepashchuk et al. (2005) satisfy the second restriction. Great care must be taken when deriving and interpreting the behavior of these absorption features (Barnes et al. 2006). The heating of the donor surface revealed by Cherepashchuk et al. (2005) makes the task even more complicated.

In SS433, the optical star loses matter both via the Roche lobe overflow and a strong stellar wind. Matter that goes through the inner Lagrangian point forms an accretion disk around the compact object, which eventually becomes geometrically thick because of strong super-Eddington accretion (see e.g. Abramowicz 2004, and references therein). Both simple estimates and more detailed calculations show that this geometrically thick accretion disk should have a height comparable to its radius $H/R \sim 1$ (e.g. Okuda et al. 2005; Nazarenko & Glazunova 2005).

The observational appearance of SS433 in X-rays is determined by multi-temperature optically thin thermal plasma emission of the jet. The X-ray emission from SS433 is subjected to both systematic and chaotic variations. Chaotic variations are likely to be caused by self-similar variability in the instantaneous mass accretion rate in the disk (Revnivtsev et al. 2005). Systematic variations in X-ray luminosity and spectral shape are determined by precessional (phases ψ) and orbital (phases ϕ) motions in the binary system.

Orbital variations are not strong, except for the eclipse. In contrast, the precessional variations are much more pronounced. In order to demonstrate this, we plot the temperature of the X-ray emission in Fig. 2 as a function of precessional and orbital phases. As the X-ray emission of SS433 is essentially multi-temperature, we considered only the high-energy part of the spectrum (10–25 keV) that probes the hottest, innermost regions of the X-ray jet. The presented temperatures are best-fit parameters of the bremsstrahlung model describing the observed spectra of SS433 in energy band 10–25 keV. Broad-band X-ray spectra of SS433 at different precessional phases are shown in Fig. 3. To demonstrate orbital variations, we have chosen the interval of precessional phases $\psi = [-0.06, 0.06]$ (the maximum disk opening phase). For precessional variations, only orbital phases $\phi = [0.3, 0.7]$ (the off-eclipse phases) have been selected.

It is seen that the best-fit temperature does not exhibit any correlation with the orbital phase except the X-ray eclipse (from $\phi \sim -0.15$ to $\phi \sim 0.15$), while strongly correlating with the precessional phase.

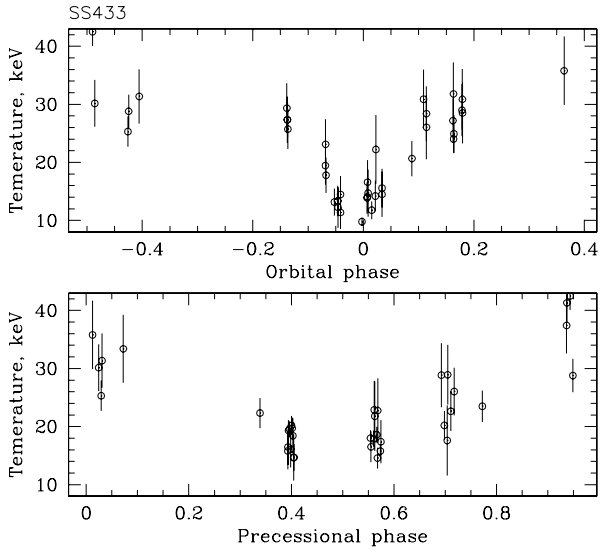

Fig. 2. The temperature of optically thin thermal plasma (bremsstrahlung fit to the 10–25 keV RXTE/PCA data) emission observed from SS433 as a function of orbital and precessional phases.

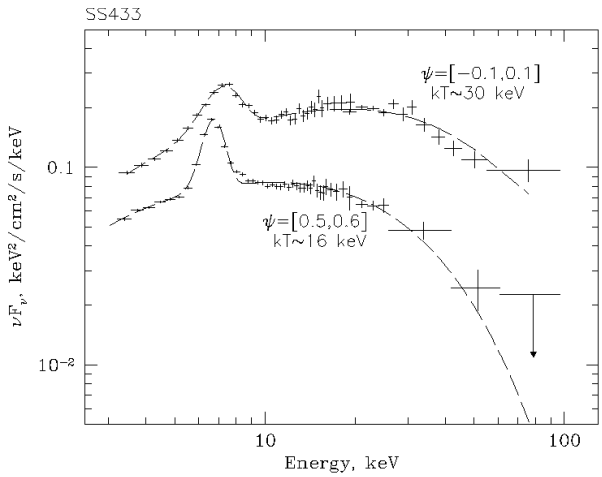

Fig. 3. Typical spectra of SS433 taken at two different disk precession phases. Only off-eclipse orbital phases $\phi = [0.3{-}0.7]$ are selected for this plot. The dashed curves show the fit by the bremsstrahlung model with broad Gaussian line profile. The best-fit values of the plasma temperature are quoted.

Note that, even at very close both precessional and orbital phases, there are statistically significant differences in the maximum jet temperatures. These temperature variations might be caused either by the nodding motion of the geometrically thick accretion disk or by chaotic (red noise) variations in the physical parameters of the plasma in the jet, similar to red-noise variations observed in the integrated X-ray flux (Revnivtsev et al. 2005).

4. The inner jet tomography by orbital and precessional eclipses

The precessional motion of the geometrically thick accretion disk causes partial obscuration of the jets. The upper jet (see Fig. 1) is least eclipsed near the precessional phase $\psi = 0.0$ (i.e. at the maximum disk opening when the upper jet points towards the observer) and is most eclipsed at $\psi = 0.5$ (i.e. when the upper jet points away from the observer). Between precessional phases $\psi \sim 0.33$ and $\psi \sim 0.66$ (the disk "edge-on" or "crossover" phases), it is the opposite (lower) jet that dominates the X-ray emission because it is directed towards the observer at these phases.

The jet eclipses caused by the optical star and/or accretion disk leads to temperature variations of the observed X-ray emission. Thus, by examining differences between spectra taken during eclipses and off eclipses we can find the spectral contribution from the innermost (hottest) regions of the jet.

In Fig. 4 we present two spectra of the jet in SS433. In the left panel (a), we plot the difference between spectra taken during the primary eclipse at $\phi = 0.021$ MJD 53 581.89 and immediately after the eclipse at $\phi = 0.114$ MJD 53 582.94 (open circles), together with off-eclipse spectrum at $\phi = 0.114$ (crosses). The spectra were accumulated over the 1024-s periods. Observations were done during the $\psi \sim 0$ disk precessional phase. In the right panel (b), we show the difference between spectra taken at precessional phases $\psi = 0$ (MJD 53 076.85) and $\psi = 0.4$ (MJD 50 878.98)[1] together with spectrum at $\psi = 0$. The curves show best-fit bremsstrahlung plus photoabsorption models to the data in the 3–5 and 11–25 keV bands where powerful emission lines do not contribute significantly. The dotted curves show bremsstrahlung models with a conventional photoabsorption column density of $N_{\rm H} = 10^{22}$ cm^{-2} (e.g. Kawai et al. 1989).

The high energy parts (11–25 keV) of the "differential" and time averaged spectra of SS433 are almost identical because they both are determined mainly by emission from the hottest parts of the jet. However, a strong photoabsorption is observed near the orbital eclipse (the left panel of Fig. 4). The best-fit value of the absorption column density in this spectrum is $N_{\rm H} = (12.5 \pm 1.5) \times 10^{22}$ cm^{-2}, much higher than the conventional value.

The spectrum of the hottest (innermost) part of the jet as derived from precessional variations off the primary eclipse (the right panel of Fig. 4) also suggests some photoabsorption, but with a considerably lowler value – here the best-fit absorbing column density is $N_{\rm H} = (4.5 \pm 1.5) \times 10^{22}$ cm^{-2}.

As a result the "differential" X-ray spectra of SS433 indicate the presence of an absorbing material in the SS433 binary system. Close to the companion star the density of this absorbing material is very high, so that the line of sight close to the stellar surface becomes practically Compton thick ($N_{\rm H} > 10^{23}$ cm^{-2}). Note that signatures of absorbing material near the optical star have previously been obtained from studies of optical absorption lines (Fabrika 1997; Fabrika et al. 1997). These studies revealed a significant strengthening in blue-shifted absorption components of P Cyg-like line profiles at orbital phases close to the primary eclipse.

The presence of such a dense absorbing material near the stellar surface can be the signature of a powerful wind from the optical star. In order to estimate the possible increase in the eclipsing region radius with respect to the star's photosphere (in our case with respect to the Roche lobe size of the star) due to the donor stellar wind, we adopted the wind model of a single *A* supergiant and took parameters of the stellar wind (its mass loss rate and the terminal velocity) from the work of Achmad et al. (1997). From observations and theoretical models, it follows that the mass loss rate of an *A* supergiant strongly depends on the mass of the star and its effective temperature and varies from $\sim 10^{-9}$ $M_\odot$/yr to $\sim 10^{-6}$ $M_\odot$/yr. The observed values of the

[1] These two observations were performed during different high-voltage epochs of the PCA. We recalculated them to a single response matrix. Both spectra were taken off the orbital eclipses.

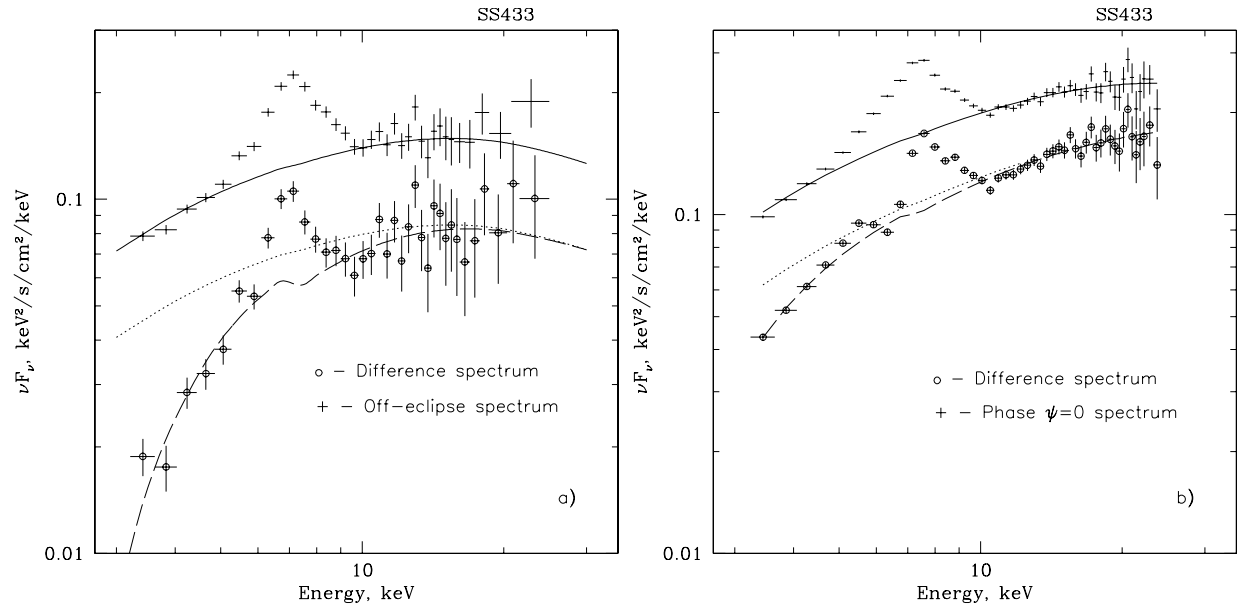

Fig. 4. a) The X-ray spectrum of SS433 immediately after the eclipse (the orbital phase $\phi = 0.114$, crosses) and the spectrum from the inner part of the jet obtained by subtracting the spectrum taken at $\phi = 0.021$ from that at $\phi = 0.114$. **b)** The X-ray spectrum of SS433 at precessional phase $\psi \sim 0$ and the difference between this spectrum and that one at $\psi \sim 0.4$ (both spectra were collected over off-eclipse orbital phases). Solid curves show thermal bremsstrahlung models with photoabsorption fitted to the data in the 3–5 and 11–25 keV bands. Dotted curves show best-fit bremsstrahlung models to the "differential" spectra with a nominal photoabsorption column density of $N_{\rm H} = 10^{22}$ cm^{-2}.

terminal velocity lie in the range 120–200 km s^{-1}. For the velocity law we use the formula

$$v(r) = v_\infty(1 - R_{\rm star}/r)^\beta$$

where $\beta = 0.8$ (Achmad et al. 1997), v_∞ is the wind terminal velocity, $R_{\rm star}$ the star radius, and r the distance from the companion star. From the mass conservation law, we get a formula for the wind density $n(r)$:

$$n(r) = \frac{n_0(1 - R_{\rm star}/a)^\beta}{(r/a)^2(1 - R_{\rm star}/r)^\beta}$$

where n_0 is the number density at the distance a from the star. We assume that the line of sight in which the column density of the stellar wind matter is higher than $N_{\rm H} > 10^{24}$ cm^{-2} is opaque for X-rays. As the spectral type and the mass of the optical star are not known exactly in the case of SS4333, we consider several cases and obtain the following results. The maximal observed value of mass outflow $\dot{M} = 8 \times 10^{-7}\ M_\odot$/yr (for star type A1 Iae, Achmad et al. 1997) results in an increase in the X-ray opaque size of the star up to 10%. The maximal theoretical value $\dot{M} = 10^{-6}\ M_\odot$/yr will lead to a 20% increase in the X-ray opaque size of the star.

Absorption in the inner dense stellar wind material weakens the assumption that the Roche lobe size of the secondary is a good measure of its X-ray opaque size. Note that the X-ray photoabsorption described above should not be visible in the time-averaged spectrum of SS433 because only emission from the hottest innermost parts of the jet are screened/absorbed, while outer cooler parts of the jet, which contribute most to the emission at energies <3–5 keV where the RXTE spectra are most sensitive to absorption, are located much farther away from the star and, hence X-ray emission from these parts is virtually unabsorbed.

5. Jet eclipses by the thick disk

Eclipses of the X-ray jet by a thick disk is a geometrical effect that depends only on the orientation of the disk changing with the precessional phase. Therefore, assuming some reasonable geometry of the thick disk, observations of SS433 at different precessional phases can be used to derive emission parameter profiles along the jet.

5.1. The structure of jets

We consider the jets in SS433 as conical plasma flows with constant velocity $v_j = 0.26\,c$ along the jet axis. In the direction perpendicular to the jet axis, matter moves with a constant velocity. We assume that the jet is uniform in the direction perpendicular to the jet axis.

The plasma flow forms a cone with constant opening angle 2θ. The radius of the jet cross section is $r = r_b + \theta l$, where r_b is the radius of the jet near the compact object[2] and l the distance from the compact object along the jet axis. The value of the cone's half-opening angle $\theta = 0.61°$ is taken from Marshall et al. (2002).

The jet plasma cools due to adiabatic expansion and radiation losses. When radiation losses become the dominant mechanism of plasma cooling, thermal instability starts to develop. In this case the temperature decreases much more rapidly than in the case of purely adiabatic expansion (e.g. Brinkmann et al. 1991). Analysis of the 0.5–10 keV X-ray emission of SS433 with high-energy resolution gratings of *Chandra* suggests that this instability does not develop, at least not when the temperature of the plasma exceeds $kT \sim 0.5$ keV (Marshall et al. 2002). Therefore we assume that the dominant cooling process in our

[2] This analytical description does not mean that the jet should start near the compact object.

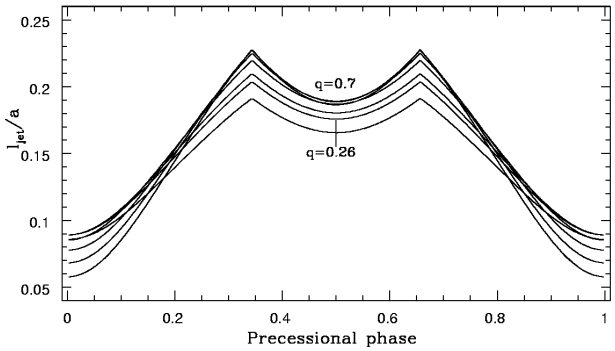

Fig. 5. The length of the invisible (eclipsed by the disk) part of the jet as a function of the precessional phase for $q = 0.2–0.7$.

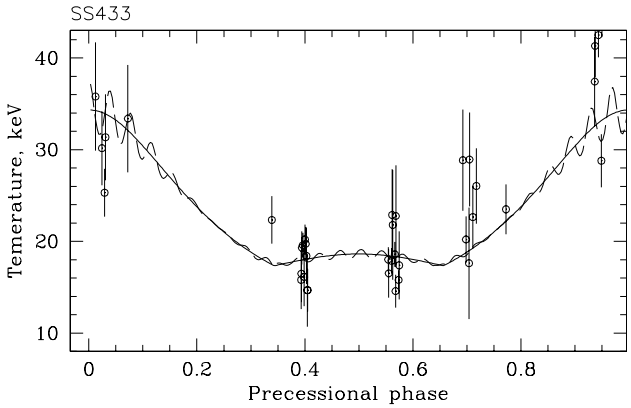

Fig. 6. The plasma temperature as a function of the precessional phase. The solid curve shows the model of adiabatic cooling of plasma moving within the cone with a constant opening angle. The dashed curve shows the same model but with a nodding motion of thick accretion disk included.

case (especially in the hottest parts of the jet of interest here) is adiabatic cooling and we can write

$$\frac{3}{2}\frac{\mathrm{d}T}{T} = \frac{\mathrm{d}V}{V} = -\frac{2\mathrm{d}r}{r}.$$

For adiabatically cooling plasma moving with a constant jet opening angle, the plasma temperature T changes with distance from the compact object l as

$$\frac{T}{T_0} = \left(1 + \theta\frac{(l - l_0)}{r_0}\right)^{-4/3}, \quad (1)$$

where T_0 is the plasma temperature and r_0 the jet cross section radius at some distance l_0 from the central source (see also Koval' & Shakura 1989; Brinkmann et al. 1991; Kotani et al. 1996).

5.2. Precession of the geometrically thick disk

The Roche lobe only loosely constrains the accretion disk radius. For a disk lying in the orbital plane, one usually adopts Paczynsky's tidal truncation radius as a measure of the outer disk radius. The accretion disk in SS433 is tilted to the orbital plane and precesses, so its outer radius can differ from Paczynsky's estimate. However, according to some numerical models (e.g. Nazarenko & Glazunova 2005), this difference is not very significant, so it will be sufficient for our purposes of adopting the disk truncation radius given by Paczynski (1977):

$$\frac{R_{\rm disk}}{a} = 0.112 + \frac{0.27}{(1 + q^{-1})} + \frac{0.239}{(1 + q^{-1})^2}.$$

For a geometrically thick disk ($H/R \sim 1$) and with the understanding that it should not overfill the Roche lobe of the compact star, we find

$$H_{\rm disk} \lesssim \left(R^2_{\rm RocheBH} - R^2_{\rm disk}\right)^{1/2},$$

where the formula for $R_{\rm RocheBH}$ is adopted from Eggleton 1983):

$$\frac{R_{\rm RocheBH}}{a} = \frac{0.49q^{2/3}}{0.6q^{2/3} + \ln(1 + q^{1/3})}.$$

In Fig. 5 we plot the distance of the nearest visible jet points from the central source as a function of the disk precessional phase for different binary mass ratios q. The mass ratio is still debatable on different grounds (see discussion above), so in the present study we varied the value of q in the range 0.2–0.7.

Using the formula (1), for given parameters $q, H_{\rm disk}$, and $R_{\rm disk}$, we can calculate the maximum model temperature of the jet visible at different precessional phases. Note that at precessional phase intervals [0, 0.33] and [0.33, 0.66] the maximum emission is provided by different jets (upper or lower). Here and below all detectable parameters are calculated in the observer's reference frame, while physical parameters of the jet are given in the jet's rest frame.

Comparing the profiles of the maximum visible temperatures derived above with observational data points enables us to find the model parameters (see Fig. 2). The best-fit parameters of our model are: $l_0/a = 0.06–0.09$ (depending on the assumed value of q), $T_0 = 30 \pm 2$ keV, and $r_0/a = (1–1.6) \times 10^{-2}$ for the jet opening angle $\theta = 0.61°$. The best-fit model is shown in Fig. 6. The limited accuracy of the temperature measurements and incomplete coverage of the precessional and nutational periods by observations preclude us from implementing the disk nodding motion in the model. For illustrative purposes, in Fig. 6 we also show the effect of the nutational variability by the dashed curve.

6. Eclipses by the optical companion

The X-ray orbital eclipses observed in SS433 are widely used to constrain the geometry of the binary system (e.g. Stewart et al. 1987; Kawai et al. 1989).

Analysis of X-ray eclipses observed at the disk maximum opening (the precessional phases $\psi \sim 0.0$) allows us to get the lower limit on the component mass ratio in SS433 independently of the (still controversial) radial velocity measurements provided by optical spectroscopy. Indeed, assuming the jet to be infinitely thin in comparison with the optical star, the duration of the X-ray eclipse yields only an upper limit on the size of the optical star (however, see the above discussion about the likely increase in the X-ray opaque size of the secondary star due to its stellar wind).

On the other hand, the examination of X-ray eclipses seen at the disk's "edge-on" precessional phases $\psi \sim 0.33$ or $\psi \sim 0.66$ (the so-called "crossover", because at that time the line of sight velocities of both jets are equal and jets lie exactly on the plane of the sky) gives us an estimate of the star radius in comparison with the accretion disk thickness. For orbital X-ray eclipses to exist in this precessional phase, the image of the star on the plane of the sky should not be embedded in the image of the thick disk on the plane of the sky. Potentially this might give us an upper limit for the value of q.

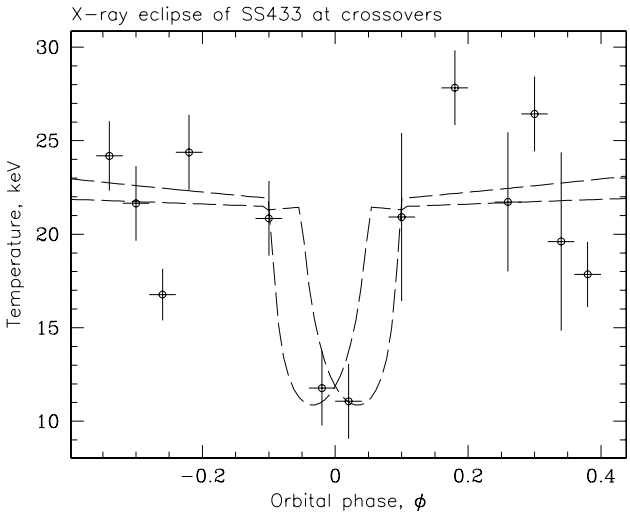

Fig. 7. Orbital X-ray eclipse of SS433 observed during the "crossover" precessional phases $|\psi - 0.33| < 0.07$ and $|\psi - 0.66| < 0.07$. Dashed lines show temperature profiles obtained in our model.

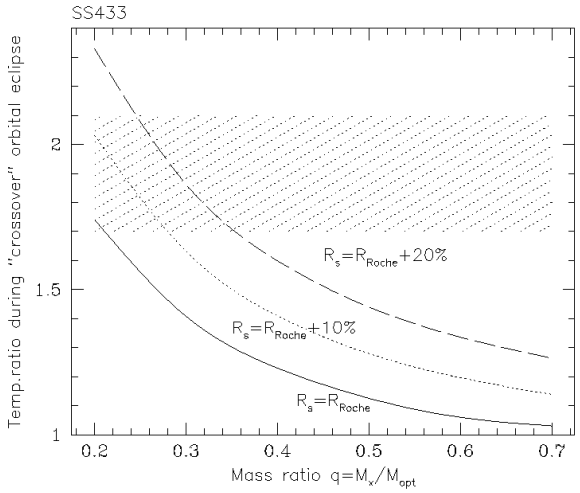

Fig. 8. The ratio of the maximum visible jet temperatures during the orbital eclipse in the "crossover" precessional phases $\psi \sim 0.33, 0.66$ as a function of the mass ratio q. The solid line is obtained for the star exactly filling its Roche lobe $R = R_{\rm Roche}$, while the dotted and dashed lines show the model with the 10% and 20% oversized star, respectively. The hatched area shows the observational constraints on the temperature ratio.

6.1. The "crossover" X-ray eclipses

In Fig. 7 we present the profile of the maximum X-ray temperature measured in the orbital eclipse near precessional phases $\psi \sim 0.33$ and 0.66. Observations with $\Delta\psi = \pm 0.07$ around phases of the exact "crossover" were selected. The orbital X-ray eclipse is clearly visible and shows an appreciable depth. The ratio of the maximum jet temperature derived from off-eclipse observations to that of the eclipsed jet is $\sim 1.9 \pm 0.2$. Dashed lines in the figure show examples of the jet maximum visible temperature profiles in the eclipse at precessional phases $\psi = 0.33$ and $\psi = 0.66$ obtained in our model. The temperature profile along the jet was taken as derived in the previous section. The mass ratio $q = 0.2$ was adopted here for clarity, and also we assumed that the size of the star is 10% larger than its Roche lobe. We have not attempted to best-fit the observed points as they were collected during observations performed at different nutational and precessional phases. Note that the model X-ray eclipse profiles during crossovers are not symmetric. This happens because the jets in these two cases are inclined differently with respect to the binary orbital plane.

The ratio of the maximum jet temperatures in the eclipse and off the eclipse is plotted in Fig. 8 as a function of the binary mass ratio q. The solid curve shows the ratio obtained under the assumption that the size of the star equals the volume-averaged radius of the Roche lobe. The value of q affects the depth of the "crossover" eclipse via the size (thickness) of the accretion disk and the secondary star.

We have shown in Sect. 4 that the assumption that the Roche lobe size of the secondary is a good measure of the X-ray opaque size of the star might be wrong due to absorption in the inner, dense stellar-wind material. Therefore in Fig. 8 we also show models of the ratio of maximum jet temperatures in and out of the eclipse assuming the star radius to be $R = 1.1 R_{\rm Roche}$ and $R = 1.2 R_{\rm Roche}$ by the dotted and dashed lines correspondingly (see discussion in Sect. 4).

From Fig. 8 we can conclude that the binary mass ratio in SS433 cannot be directly determined from the depth or duration of the X-ray eclipses. The result depends on the extent of the eclipsing region over the stellar Roche lobe. However, if the binary mass ratio is significantly higher than $q \sim 0.3$–0.35, the eclipsing region size seems to be too big, $R \gg 1.2 R_{\rm Roche}$, which is not very likely. Comparison of the observed temperature ratio with our model suggests that the X-ray opaque size of the star should be larger than $R/a \gtrsim 0.5$–0.55.

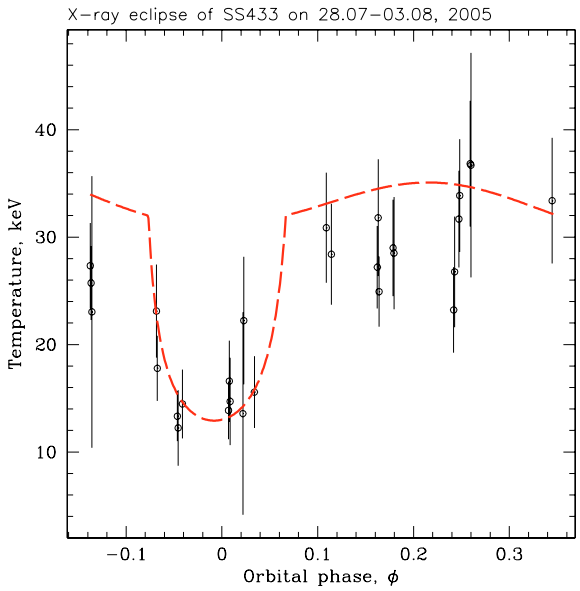

Fig. 9. The jet eclipse profile by the optical companion for $q = 0.26$. The dashed line shows the best-fit model.

6.2. X-ray eclipse at $\psi \sim 0$

In order to obtain a high quality profile of the jet maximum temperature across a single eclipse, we performed a set of dedicated RXTE observations of SS433 on July 28–Aug. 3, 2005 near the precessional phase $\psi \sim 0$. The temperature profile obtained from these observations is presented in Fig. 9. Using the temperature distribution along the jet length l derived in the previous section, we calculated the expected behavior of the maximum jet temperature during the eclipse for different sizes of the eclipsing region R.

The comparison of the model with obtained data points yielded the best-fit value $R/a = 0.53 \pm 0.02$ ($\chi^2 = 34$ for 24 degrees of freedom) for $q = 0.26$, which is ∼7% higher than the size of the Roche lobe of the secondary would have at such q. The best-fit model is shown in Fig. 9. For demonstration purposes we included the effect of accretion disk nodding motion in the model.

It is interesting to note that the quality of the fit can be improved if we assume a non-spherical shape of the eclipsing region (star plus inner wind). This is a plausible geometry if the wind density from equatorial regions of the star is higher than from polar regions.

7. Conclusion

X-ray emission of SS433 demonstrates both chaotic (aperiodic) and periodic variations. In this paper, we used extensive observational data obtained by RXTE to studing systematic variations in the X-ray emission of SS433 caused by precessional and orbital motions in the system.

- By comparing X-ray spectra of SS433 near and in the eclipse, we obtained strong signatures of a significant ($N_{\rm H} > 10^{23}$ cm^{-2}) photoabsorption of X-rays near the companion star. We argue that this might be caused by the presence of a dense stellar wind from the companion star. The mass loss rate in the wind needed to explain the observed photoabsortion is $\dot{M} \sim 10^{-6}\ M_\odot$/yr.
- From detection of strong photoabsorption near the secondary star, we conclude that the X-ray opaque size of the secondary might be significantly larger than the Roche lobe size of the star. Therefore one should be cautious when estimating the Roche lobe size of the secondary from X-ray orbital eclipses.
- By both assuming the shape of the geometrically-thick accretion disk restricted by the Roche lobe size of the compact star and using the RXTE observations of SS433 at different precessional phases, we recovered the temperature profile of plasma along the jet. The obtained maximum temperature visible in the jet is $T \sim 30$ keV at a distance of $l/a = 0.06–0.09$ from the compact object. The radius of the jet at this distance is $r_0/a = 0.01–0.016$. Here the jet was assumed to have a constant opening angle.
- We reliably detected orbital X-ray eclipses in SS433 during the "crossover" precessional phases when the X-ray jets and the axis of the accretion disk lie exactly on the plane of the sky. The observed depth of the X-ray eclipse combined with our assumptions about the accretion disk thickness implies that the size of the star is larger than $R/a \gtrsim 0.5$, yielding an upper bound on the mass ratio of the components in SS433 $q < 0.3–0.35$, assuming that the radius of the eclipsing region (star plus inner wind) cannot be much larger than $1.2R_{\rm Roche,secondary}$.

Acknowledgements. Authors are grateful to the anonymous referee for very valuable remarks, which helped to improve the manuscript. This research made use of data obtained from High Energy Astrophysics Science Archive Research Center Online Service, provided by the NASA/Goddard Space Flight Center. This work was supported by RFBR grants Nos 04-02-16349, 05-02-19710, 06-02-16025, 04-02-17276, and 04-02-16720, and by joint RFBR/JSPS grant No 05-02-12710.

References

Abramowicz, M. 2004, [arXiv:astro-ph/0411185]
Achmad, L., Lamers, H. J. G. L. M., & Pasquini, L. 1997, A&A, 320, 196
Antokhina, É. A., Seifina, E. V., & Cherepashchuk, A. M. 1992, SvA, 36, 143
Barnes, A. D., Casares, J., Charles, P. A., et al. 2006, MNRAS, 365, 296
Brinkmann, W., Kawai, N., Matsuoka, M., & Fink, H. H. 1991, A&A, 241, 112
Cherepaschuk, A. 2002, Space Sci. Rev., 102, 23
Cherepashchuk, A. M., Sunyaev, R. A., Seifina, E. V., et al. 2003, A&A, 411, L441
Cherepashchuk, A. M., Sunyaev, R. A., Fabrika, S. N., et al. 2005, A&A, 437, 561
Dolan, J. F., Boyd, P. T., Fabrika, S., et al. 1997, A&A, 327, 648
Eggleton, P. P. 1983, ApJ, 268, 368
Fabrika, S. N. 1997, Ap&SS, 252, 439
Fabrika, S. 2004, Astrophys. Sp. Phys. Rev., 12, 1
Fabrika, S. N., Goranskij, V. P., Rakhimov, V. Y., et al. 1997, BSAO, 43, 109
Gies, D. R., Huang, W., & McSwain, M. V. 2002a, ApJ, 578, L67
Gies, D. R., McSwain, M. V., Riddle, R. L., et al. 2002b, ApJ, 566, 1069
Hillwig, T. C., Gies, D. R., Huang, W., et al. 2004, ApJ, 615, 422
Jahoda, K., Markwardt, C. B., Radeva, Y., et al. 2006, ApJS, 163, 401
Kawai, N., Matsuoka, M., Pan, H., & Stewart, G. C. 1989, PASJ, 41, 491
Kotani, T., Kawai, N., Matsuoka, M., & Brinkmann, W. 1996, PASJ, 48, 619
Koval', E., & Shakura, N. 1989, in Proc. 23rd ESLAB Symp. on Two- Topics in X-ray Astronomy, ESA SP-296, 479
Margon, B. 1984, ARA&A, 22, 507
Marshall, F. E., Swank, J. H., Boldt, E. A., Holt, S. S., & Serlemitsos, P. J. 1979, ApJ, 230, L1
Marshall, H. L., Canizares, C. R., & Schulz, N. S. 2002, ApJ, 564, 941
Matsuoka, M., Takano, S., Makishima, K. 1986, MNRAS, 222, 605
Namiki, M., Kawai, N., Kotani, T., & Makishima, K. 2003, PASJ, 55, 281
Nandi, A., Chakrabarti, S., Belloni, T., & Goldoni, P. 2005, MNRAS, 359, 629
Nazarenko, V. V., & Glazunova, L. V. 2005, ARep, 49, 826
Okuda, T., Teresi, V., Toscano, E., & Molteni, D. 2005, MNRAS, 357, 295
Paczynski, B. 1977, ApJ, 216, 822
Revnivtsev, M., et al. 2005, A&A, 447, 545
Stewart, G. C., Watson, M. G., Matsuoka, M., et al. 1987, MNRAS, 228, 293
Watson, M., Stewart, G., Brinkmann, W., & King, A. 1986, MNRAS, 222, 261
Yuan, W., Kawai, N., Brinkmann, W., & Matsuoka, M. 1995, A&A, 297, 451